ELSEVIER

Journal of Crystal Growth 187 (1998) 289–302

JOURNAL OF CRYSTAL GROWTH

A diffusion boundary layer model of microsegregation

X. Tong, C. Beckermann*

Department of Mechanical Engineering, The University of Iowa, Iowa City, IA 52242, USA

Received 24 April 1997; accepted 20 September 1997

Abstract

A microsegregation model, based on a boundary layer concept, is proposed for solidification of alloys. The model is derived by considering finite-rate solute diffusion both in the liquid and in the solid. A solutal Fourier number is used to characterize the extent of finite-rate solute diffusion in the liquid phase ahead of the moving solid/liquid interface. This new parameter is the liquid counterpart of the solutal Fourier number in the solid phase used before to characterize finite-rate back-diffusion in the solid. It can be obtained through the knowledge of either the local solidification time or the operating point of the cell/dendrite tip (among other parameters). The present microsegregation model covers the entire spectrum of solidification rates, up to the limit of a microsegregation free solid. The model predictions show good agreement with a previous rapid solidification experiment involving an Ag–Cu alloy. Also, a new relation is derived for the primary dendrite arm spacing.

1. Introduction

Microsegregation models are an indispensable part of analyzing alloy solidification phenomena, and a detailed review of the numerous available models can be found in the literature [1]. The well-known lever rule and Scheil equation [2–4], the Brody–Flemings model [5] as well as more recent models due to Clyne and Kurz [6], Ohnaka [7], and Kobayashi [8] all assume that the liquid between the dendrites or cells is solutally well-mixed and cell/dendrite tip undercooling is not considered. They differ only in the way solute back-diffusion in the solid phase is modeled.

Several models have been devised to take into account the solute concentration gradients in the liquid [1], which are of primary importance in rapid solidification [9–11]. The first such analysis was presented by Bower et al. [12], who considered finite rate solute diffusion in the liquid parallel to the primary growth direction. The liquid concentration was assumed to be uniform between neighboring cells or dendrites, perpendicular to the growth direction. Solari and Biloni [13] used the model of Burden and Hunt [14] to include the important effect of cell or dendrite tip undercooling due to solute concentration gradients in the liquid ahead of the tips. It should be noted, however, that the Burden and Hunt model is only applicable at low and medium growth rates. A simpler approach was proposed by Flood and Hunt [15] to take into account the dendrite tip undercooling. In their

* Corresponding author.

0022-0248/98/$19.00
PII S0022-0248(97)00878-6

so-called "truncated Scheil" method, the depression of the dendrite tip temperature due to finite rate solute diffusion in the liquid is calculated from any of the available dendrite tip growth models (such as the ones by Burden and Hunt [14] or Kurz et al. [16]). Using then this tip temperature in a standard Scheil analysis results in a jump in the solid fraction from zero to some finite value at the dendrite tip. Behind the tip, the solid fraction continues to be calculated from the Scheil equation. Kattner et al. [17] recently modified this model to conserve solute. Giovanola and Kurz [18,19] proposed a so-called patching method which considers the mushy zone as two sub-regions: a solutally well-mixed region for solid volume fractions larger than some prescribed value, and a near-tip region where the liquid is undercooled. For the well-mixed region, either the Scheil model or the Brody–Flemings model is used, while for the near-tip region a quadratic curve fit is used to relate the local solid fraction to the interfacial concentration. The Giovanola and Kurz model gives good agreement with experimental results, as shown by Giovanola and Kurz [18,19] and Flemings [20]. Wang and Beckermann [21] proposed a model which consists of a set of ordinary differential equations for the micro-scale diffusion processes in both the solid and the liquid. Their model was derived from a volume averaging approach. For rapid solidification, the model equations become rather stiff, and special solution methods, such as Gear's method, are necessary. Nonetheless, it also gives good agreement with the experimental results. There are also available a number of numerical approaches for calculating the effect of finite-rate solute diffusion, the most recent and advanced being the studies by Lu and Hunt [22,23]. They considered two-dimensional solute diffusion in the liquid, and provided predictions of the cell or dendrite tip undercooling, shape and spacing for all growth rates. Although analytical curve fits were provided for the cell and dendrite spacings in terms of relevant dimensionless parameters [23], the full model would be too cumbersome to use for microsegregation predictions in a combined heat transfer-solidification analysis of a casting. Spencer and Huppert [24] recently presented an asymptotic theory for directional solidification of slender needle crystals. Their analysis results in an integral equation for the shape of the needle crystal, in addition to the solute profiles. An interesting result is that the tip radius and array spacing are closely related, which is in contrast to the traditional tip selection theories for free dendritic growth that are based on surface energy only.

The objective of the present study is to develop a physically sound microsegregation model, based on a boundary layer concept, which can be easily applied to rapid solidification processes and also reduces to a standard back-diffusion model at lower solidification rates. The distinguishing feature of this analytical model is that it considers finite-rate solute diffusion in the liquid in the direction perpendicular to the cell or dendrite axis. An asymptotic analysis is presented that allows for a prediction of the cell/dendrite tip operating point. The model is fine-tuned through a comparison with results from a numerical solution of the diffusion equation. It is validated through comparison with other theoretical and experimental results. Finally, it is shown how the present model can be used to calculate the primary dendrite arm spacing.

2. Model formulation

Following similar arguments as by Lu and Hunt [22,23], the effects of the packing geometry of the cell or dendrite array and the presence of dendrite side arms are neglected. Heat flow is assumed to be unidirectional along the growth axis. As illustrated in Fig. 1, a solute boundary layer develops in the liquid along a growing cell or dendrite surface. The liquid concentration varies from the interfacial concentration, C_l^*, to the initial concentration, C_0, across the boundary layer. The boundary layers between two neighbouring cells or dendrites grow, while the liquid space shrinks, until they meet at the symmetry line. After overlap, the liquid concentration at the symmetry line will no longer be equal to C_0. Ultimately the concentration in the liquid between the cells/dendrites becomes uniform and equal to C_l^*. The liquid concentration inside the boundary layer also varies along the growth axis, because the interfacial concentration, C_l^*, evolves

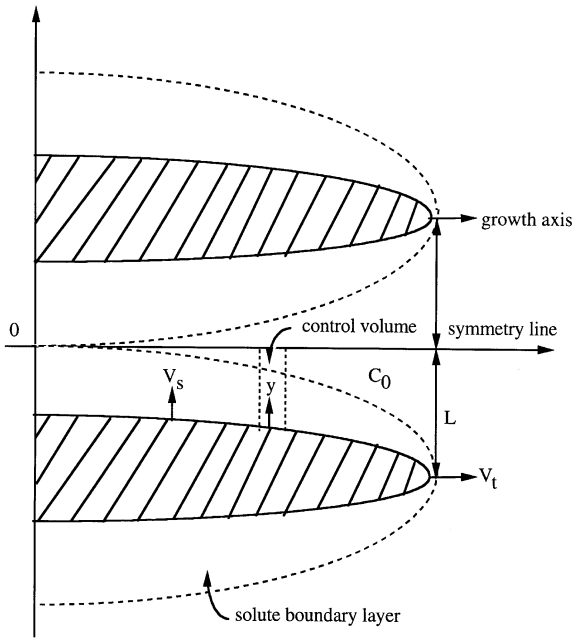

Fig. 1. Schematic of the solute diffusion boundary layer.

with temperature according to the phase diagram. Most of the early microsegregation analyses that consider solute diffusion in the liquid (see Introduction) account only for axial diffusion, and assume the liquid to be solutally well-mixed at any given axial location.

In the present study (as well as in Ref. [21]), on the other hand, liquid solute diffusion along the growth axis is neglected in comparison to lateral diffusion (across the boundary layer). This assumption is in accordance with traditional boundary layer theory [25], and can be formally verified through an order of magnitude analysis. It can be understood by realizing that the boundary layer thickness or the spacing between neighbouring cells/dendrites is much smaller than the axial distance from the tips to the roots of the cells/dendrites.

Instead of performing a full boundary layer analysis, we seek a simple integral-type solution by assuming a certain lateral liquid concentration profile. A good approximation was found to be the quasi-steady profile for one-dimensional solute diffusion ahead of a moving solid–liquid interface, i.e.,

$$\frac{C_l - C_0}{C_l^* - C_0} = \exp\left[-\frac{1}{\sigma}\frac{V_s y}{D_l} \right], \tag{1}$$

where C_l is the solute concentration in the liquid, D_l the liquid mass diffusivity, and y the coordinate moving with the cell/dendrite surface at the velocity V_s toward the symmetry line (see Fig. 1). It is important to note that both V_s and C_l^* vary along the growth axis. The interface velocity V_s is a maximum at the cell/dendrite tip and decreases toward the root. For small V_s, Eq. (1) shows that C_l approaches C_l^* everywhere. Obviously, Eq. (1) does not satisfy the zero flux condition at the symmetry line once the boundary layers meet. For this reason, as well as for possible nonquasi-steady effects, a "tuning" constant σ is included in Eq. (1). It is of the order of unity and is determined below through a comparison with a numerical solution of the unsteady, one-dimensional diffusion equation in the finite liquid space between the cells/dendrites, for which Eq. (1) is only an approximation.

Assuming a parabolic cooling law, as is commonly done in solidification analyses [18,19], the following relationship exists between the local solid fraction f_s and time t:

$$f_s = \sqrt{\frac{t}{t_f}}, \tag{2}$$

where t_f is the local solidification time [2,3]. The solid–liquid interface velocity V_s can be expressed in terms of a simple geometric relation:

$$V_s = L\frac{df_s}{dt}, \tag{3}$$

where L is half of the cell/dendrite spacing λ_1 (i.e., $L = \lambda_1/2$). Combining Eqs. (2) and (3) leads to

$$V_s = \frac{L}{2t_f f_s}. \tag{4}$$

The Fourier number for solute diffusion in the liquid, β, is defined as follows:

$$\beta = \frac{D_l t_f}{L^2} \tag{5a}$$

or for use in the following:

$$\beta' = \sigma\frac{D_l t_f}{L^2} = \sigma\beta. \tag{5b}$$

Introducing Eqs. (4) and (5b) into Eq. (1) and integrating over the liquid region, the average solute concentration in the liquid $\bar{C}_l$ is given by:

$$\frac{\bar{C}_l - C_0}{C_l^* - C_0} = \frac{1}{L(1-f_s)}\int_0^{L(1-f_s)} \exp\left(-\frac{y}{L}\frac{1}{2\beta' f_s}\right) dy$$
$$= \frac{2\beta' f_s}{1-f_s}\left[1 - \exp\left(-\frac{1-f_s}{2\beta' f_s}\right)\right]. \tag{6}$$

Eq. (6) is plotted in Fig. 2. It can be seen that $\bar{C}_l$ approaches C_l^* for large β' at all solid fractions (i.e., the liquid is solutally well-mixed), whereas $\bar{C}_l$ remains close to C_0 for $\beta' \to 0$ until f_s approaches unity. For intermediate β', the average liquid concentration between the cells/dendrites increases smoothly from C_0 to C_l^* with increasing solid fraction or distance from the tip. Note that solidification often terminates in a eutectic reaction, at which point the present model becomes inapplicable. Also shown in Fig. 2 is the solid fraction variation of the boundary layer thickness, δ, defined as the location in y where $(C_l - C_0)/(C_l^* - C_0) = 0.01$. It is nondimensionalized with the liquid spacing $L_l[= L(1-f_s)]$. The boundary layer rapidly approaches the symmetry line for $\beta' > 1$. At the solid fraction where $\delta/L_l = 1$, the boundary layers between neighbouring cells/dendrites meet and the liquid concentration at the symmetry line is no longer C_0. For $\beta' = 0.1$, this solid faction is about 0.5; hence, this case roughly corresponds to Fig. 1. For even smaller β', the boundary layer stays relatively thin for a large portion of the solid fraction range, and

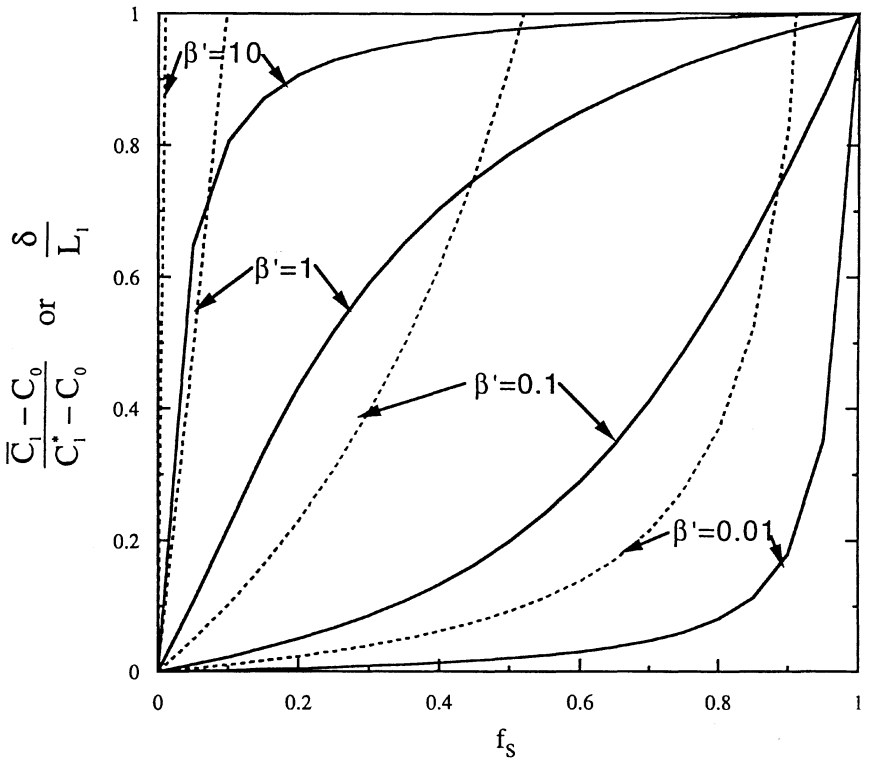

Fig. 2. Average liquid solute concentration (solid lines) and solute boundary layer thickness (dashed lines) as a function of the solid fraction for different solutal Fourier numbers, β'.

then exponentially approaches L_1 at high solid fractions.

The average liquid concentration from Eq. (6) is used in an overall solute balance, i.e.,

$$f_s\bar{C}_s + (1 - f_s)\bar{C}_l = C_0, \tag{7}$$

where equal solid and liquid densities and a closed system are assumed. The average solute concentration in the solid, $\bar{C}_s$, is obtained from the following conservation equation [21]:

$$\frac{d(f_s\bar{C}_s)}{dt} = C_s^*\frac{df_s}{dt} + \frac{D_sS_s}{l_s}(C_s^* - \bar{C}_s), \tag{8}$$

where C_s^* is the solid concentration at the interface and l_s is a so-called diffusion length in the solid. Back diffusion in the solid phase is modeled in the same way as in Ref. [21], by assuming the solute profile in the solid to be parabolic. Then, the diffusion length can be shown to be $l_s = f_sL/3$. The area concentration, S_s (solid/liquid interfacial area per unit volume), is given by $S_s = 1/L$. Hence, Eq. (8) becomes,

$$f_s\frac{d\bar{C}_s}{dt} = (1 + 6\alpha)(C_s^* - \bar{C}_s)\frac{df_s}{dt}, \tag{9}$$

where

$$\alpha = \frac{D_st_f}{L^2} \tag{10}$$

is the solutal Fourier number in the solid. Finally, C_s^* is related to C_l^* by,

$$C_s^* = kC_l^*, \tag{11}$$

where k is the partition coefficient. In rapid solidification, the partition coefficient k is often evaluated from a relation derived by Aziz [26], such that k tends to unity for a large interface speed.

Combining Eqs. (6), (7) and (9), the following first order ordinary differential equation can be derived:

$$F_1(f_s)\frac{dC_s^*}{df_s} = F_2(f_s, C_s^*), \tag{12}$$

where the functions $F_1(f_s)$ and $F_2(f_s, C_s^*)$ are given by

$$F_1(f_s) = \frac{2\beta' f_s}{k}\left[1 - \exp\left(-\frac{1 - f_s}{2\beta' f_s}\right)\right], \tag{13}$$

$$F_2(f_s, C_s^*) = (1 + 6\alpha)(C_0 - C_s^*) + \left(\frac{C_s^*}{k} - C_0\right) \times \left\{\frac{\exp[(1 - f_s)/2\beta' f_s]}{f_s} - 2\beta'(1 + 6\alpha) \times \left[1 - \exp\left(-\frac{1 - f_s}{2\beta' f_s}\right)\right]\right\}. \tag{14}$$

Eq. (12) represents the present microsegregation model. Even if the complicated forms of the functions $F_1(f_s)$ and $F_2(f_s, C_s^*)$ prevent us from obtaining an analytical solution, it can be solved very easily by means of numerical integration.

3. Results and discussion

3.1. Limiting cases

From Eq. (12), it can be seen that there are only two dimensionless parameters, α and β (or β'), which need to be specified in addition to the initial solute concentration, C_0, and the partition coefficient, k. Both dimensionless parameters are solutal Fourier numbers, but they are based on different mass diffusivities. The solid back-diffusion parameter α is not new; it appears, e.g., in the Brody–Flemings [8] and the Wang–Beckermann [21] models. The parameter β is firstly proposed in this work, and characterizes the finite rate diffusion in the *liquid* phase perpendicular to the cell/dendrite axis. The ratio of α to β equals the ratio of D_s to D_l, which is in the range of 10^{-3}–10^{-4} for most alloys (carbon in iron is an important exception). Therefore, these two parameters will not play significant roles simultaneously in predicting microsegregation patterns. In other words, when finite rate diffusion in the liquid has to be considered, e.g., in rapid solidification, the solid back-diffusion effect is negligible; on the other hand, when back diffusion in the solid becomes important, the liquid phase is already solutally well-mixed. Hence, α and β play

their respective roles at different ends of the solidification spectrum. However, the present model is able to cover the entire spectrum.

The above discussion leads to the consideration of the following limiting cases:

(i) when $\beta \to \infty$ and $\alpha \to 0$, the Scheil model is obtained:

$$F_1(f_s) \to \frac{1-f_s}{k} \quad \text{and} \quad F_2(f_s, C_s^*) \to \frac{1-k}{k} C_s^*,$$

$$\frac{dC_l^*}{df_s} - \frac{1-k}{1-f_s} C_l^* = 0. \tag{15}$$

The solution to Eq. (15) is

$$f_s = 1 - \left(\frac{C_0}{C_l^*}\right)^{1/(1-k)}, \tag{16}$$

(ii) when $\beta \to \infty$ and $\alpha \to \infty$, the lever rule is obtained:

$$C_l^* = \frac{C_0}{1-(1-k)f_s}; \tag{17}$$

(iii) when $\beta \to \infty$, Wang and Beckermann's back-diffusion model [21] is obtained:

$$F_1(f_s) \to \frac{1-f_s}{k} \quad \text{and} \quad F_2(f_s, C_s^*) \to (1+6\alpha)\frac{1-k}{k} \times C_s^* - \frac{6\alpha}{f_s}\left(\frac{C_s^*}{k} - C_0\right),$$

$$\frac{dC_l^*}{df_s} + \left[\frac{(1+6\alpha)k-1}{1-f_s} + \frac{6\alpha}{f_s}\right] C_l^* = \frac{6\alpha}{f_s(1-f_s)} C_0; \tag{18}$$

(iv) when $\beta \to 0$, a microsegregation free structure is predicted:

$$F_1(f_s) \to 0 \quad \text{and} \quad F_2(f_s, C_s^*) \to C_0 - C_s^*.$$

Thus,

$$C_s^* = C_0. \tag{19}$$

Eq. (18) has an integral solution as presented in Ref. [21]. Because back-diffusion in the solid has been thoroughly discussed in previous publications [8,10,11,21], the remainder of this article focuses on

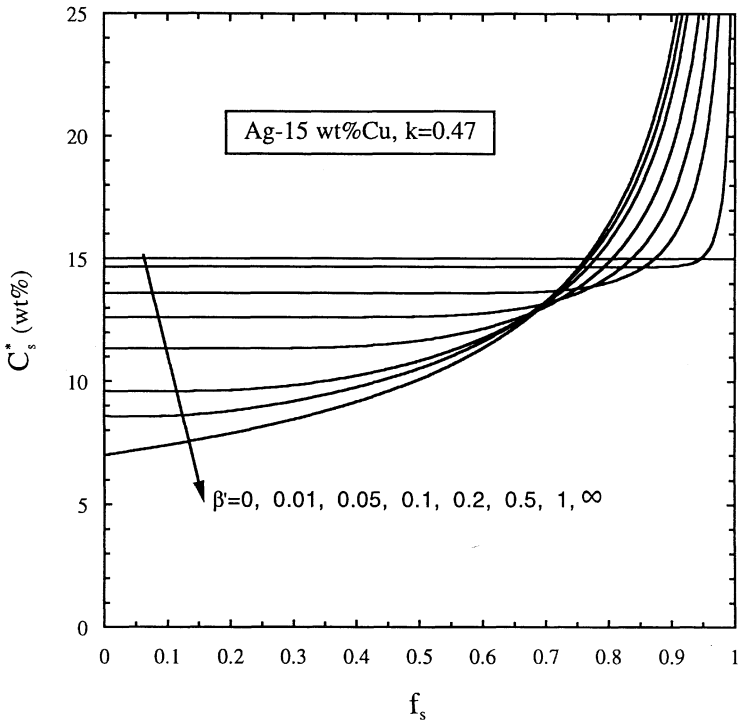

Fig. 3. Predicted microsegregation profiles as a function of the Fourier number, β' (the same partition coefficient was used for all β').

finite-rate diffusion of solute in the liquid phase only, and α is set to zero.

3.2. Numerical results

Fig. 3 shows numerical solutions of Eq. (12) for different values of β' and $\alpha = 0$. The initial concentration, C_0, and the partition coefficient, k, were set to 15 wt% and 0.47, respectively, which roughly correspond to the Ag–Cu alloy experiments of Bendersky and Boettinger [27], as is discussed in more detail below. It can be seen that a microsegregation free solute profile is obtained for $\beta' < 10^{-2}$. The Scheil predictions are approached for $\beta' > 10$. For intermediate values of β' the microsegregation profile is flat in the dendrite tip region (i.e., small f_s) and approaches a Scheil-type behavior at larger solid fractions when the liquid becomes solutally well-mixed. The value of the interfacial solid concentration, C_s^*, at vanishing solid fractions (i.e., $f_s = 0$) represents the dendrite tip operating point. This issue is analyzed in the next section. However, it can be observed that the tip concentration increases from $C_s^* = kC_0 = 7.05$ wt% to $C_s^* = C_0 = 15$ wt% with decreasing β'.

It should be mentioned that Eq. (12) was solved by the explicit Euler method [28]. The solid fraction increment used in the numerical integration was 10^{-4} for all results presented in this work. That choice of increment is rather conservative, and extensive numerical experiments showed that increasing the increment to 10^{-2} produces almost identical results.

3.3. Analysis of the tip operating point

Obviously, the solution of Eq. (12) requires an initial condition, i.e., C_s^* at $f_s = 0$. As illustrated in Fig. 4, the numerical results quickly converge to the same C_s^* curve for a given β', regardless of the initial value chosen. In other words, the microsegregation profile is a function of the parameter β' only, and the tip operating point is uniquely determined by the choice of β' for a given alloy.

This interesting, but expected, feature can be seen more readily from the following asymptotic

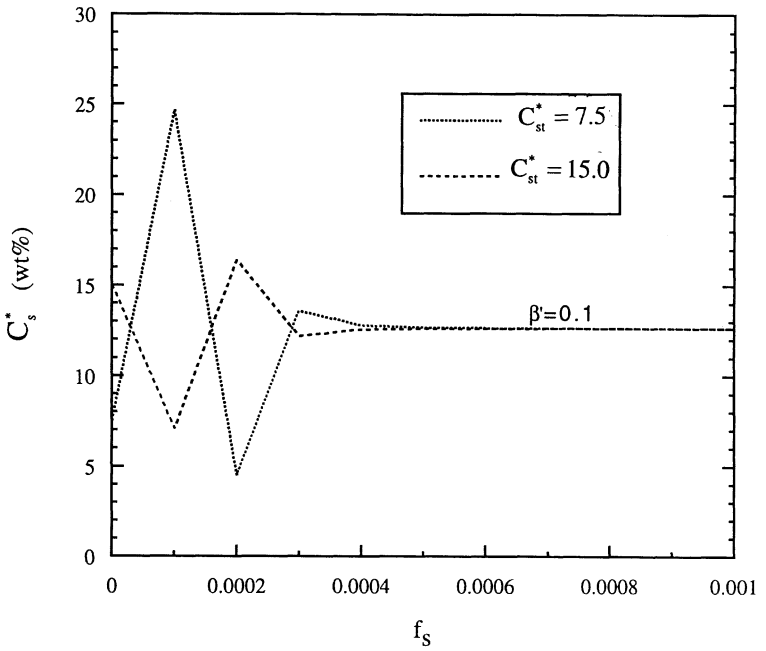

Fig. 4. Effect of the initial tip concentration on the numerical solution of Eq. (13); the solid fraction increment in the numerical solution was 0.0001; all differences due to the choice of the initial concentration disappear after the fourth step.

analysis of Eq. (12). As the solid fraction f_s approaches zero, the functions F_1 and F_2 reduce to

$$F_1(f_s) \to 0 \quad \text{and} \quad F_2(f_s, C_s^*) \to (1 + 6\alpha) \times [C_0 - C_s^* - 2\beta'(C_s^*/k - C_0)].$$

Hence, Eq. (12) becomes

$$C_{st}^* = \frac{1 + 2\beta'}{1 + 2\beta'/k} C_0 \quad (f_s = 0), \tag{20}$$

where C_{st}^* is the interfacial concentration in the solid at the dendrite tip ($f_s = 0$). To avoid numerical instabilities for small solid fractions, Eq. (20) should be used to evaluate the initial value of C_s^*. More importantly, Eq. (20) represents, in theory, a new relation for calculating the operating point (i.e., concentration) of a cell/dendrite tip. It only requires the knowledge of β', which can be estimated from its definition given by Eq. (5b). Such an estimation would involve the evaluation of the local solidification time, the cell/dendrite arm spacing, and the tuning constant σ (see the next section). Eq. (20) also shows that the tip concentration, C_{st}^*, approaches C_0 in the limits of $k \to 1$ or $\beta' \to 0$. The former occurs when $V_t \to \infty$, while the latter was already discussed in connection with Eq. (19). Both cases will be satisfied simultaneously, i.e., if $\beta' \to 0$, the tip velocity will be so large that $k \to 1$. For $\beta' \to \infty$, $C_{st}^* = kC_0$ as expected.

Traditionally, the tip operating point is determined from the following general growth law [3]:

$$C_{st}^* = \frac{kC_0}{1 - (1 - k)\mathrm{Iv}(\mathrm{Pe})}, \tag{21}$$

where Iv(Pe) is the Ivantsov function and Pe is the tip Peclet number based on the tip speed, V_t, and tip radius. Together with the marginal stability criterion [16], this model gives the correct behavior of the tip composition-growth rate relation for both low and high growth rates up to the limit of absolute stability. Combining Eqs. (20) and (21) gives a relationship between the present liquid solute diffusion parameter, β', and the tip Peclet number, Pe, as

$$\beta' = \frac{1 - \mathrm{Iv}(\mathrm{Pe})}{2\mathrm{Iv}(\mathrm{Pe})}. \tag{22}$$

Eq. (22) is plotted in Fig. 5. It can be seen that, according to the previous analysis of β', undercooling in the tip region is important only for $\mathrm{Pe} > 10^{-2}$ (i.e., when $\beta' < 10$). When $\mathrm{Pe} > 10$, the Fourier number β' is below 0.05 and a microsegregation-free structure is approached.

It is critical to note that Eq. (22) provides an alternative means of estimating the parameter β' [besides Eq. (5b)]. This alternative method does not require the knowledge of σ, t_f and L, but only of the tip Peclet number, as will be demonstrated in the validation section. Eq. (22) also establishes the connection between the present and previous analyses of microsegregation in the presence of tip undercooling.

3.4. Estimation of the tuning constant σ

The tuning constant σ was included in the parameter β' to allow for better matching of the assumed exponential solute profile in the liquid [i.e., Eq. (1)] with the actual profile, as it is present during solidification. Possible reasons for differences are manyfold and include: nonquasi-stationary behavior, the zero-flux condition at the symmetry line, multi-dimensional diffusion, unequal densities, and others. In the absence of a model that includes all of the above effects, and short of comparing directly to experimental

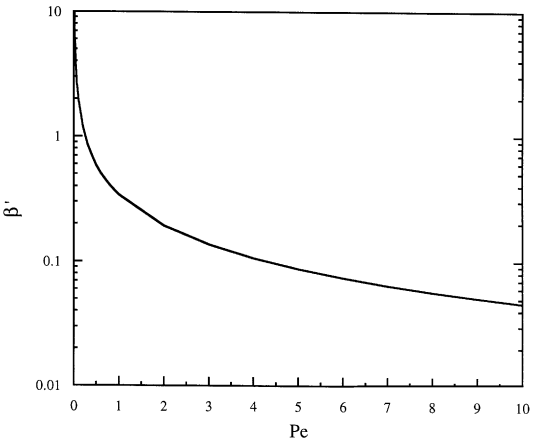

Fig. 5. Solutal Fourier number, β', as a function of the tip Peclet number, Pe.

measurements (as is done in the next section), the tuning constant σ is estimated here through a comparison with a numerical solution of the one-dimensional, unsteady diffusion equation in the finite liquid space ahead of the moving solid/liquid interface. Hence, this comparison will only remove the uncertainties associated with the first two items in the above list.

The dimensionless liquid diffusion equation and its boundary and initial conditions are

$$\frac{\partial C_l}{\partial \bar{t}} = \frac{\partial}{\partial \bar{y}}\left(\beta \frac{\partial C_l}{\partial \bar{y}}\right); \quad \bar{y}_s \leqslant \bar{y} \leqslant 1, \quad \bar{t} \geqslant 0, \tag{23}$$

$$\text{I.C.:} \quad C_l(\bar{y}, 0) = C_0, \tag{24}$$

$$\text{B.C.:} \quad C_l(\bar{y} = \bar{y}_s, \bar{t}) = C_l^*$$

$$\text{and} \quad \partial C_l(\bar{y} = 1, \bar{t})/\partial \bar{y} = 0, \tag{25}$$

where

$$\bar{y} = \frac{y}{L}, \quad \bar{t} = \frac{t}{t_f}, \tag{26}$$

and $\bar{y}_s = f_s$ is the dimensionless position of the moving solid–liquid interface. The above system of equations was mapped to a region of fixed size using a Landau transformation and solved in conjunction with Eqs. (7) and (9) (with $\alpha = 0$), and Eq. (11). Details of the numerical solution procedure can be obtained from Tong et al. [29].

Fig. 6 shows a comparison of model predictions with the numerical solution of Eq. (23) for $C_0 = 15\%$ and $k = 0.47$. By choosing an appropriate value for σ, the solute profile from the present microsegregation model [Eq. (12)] can be made to

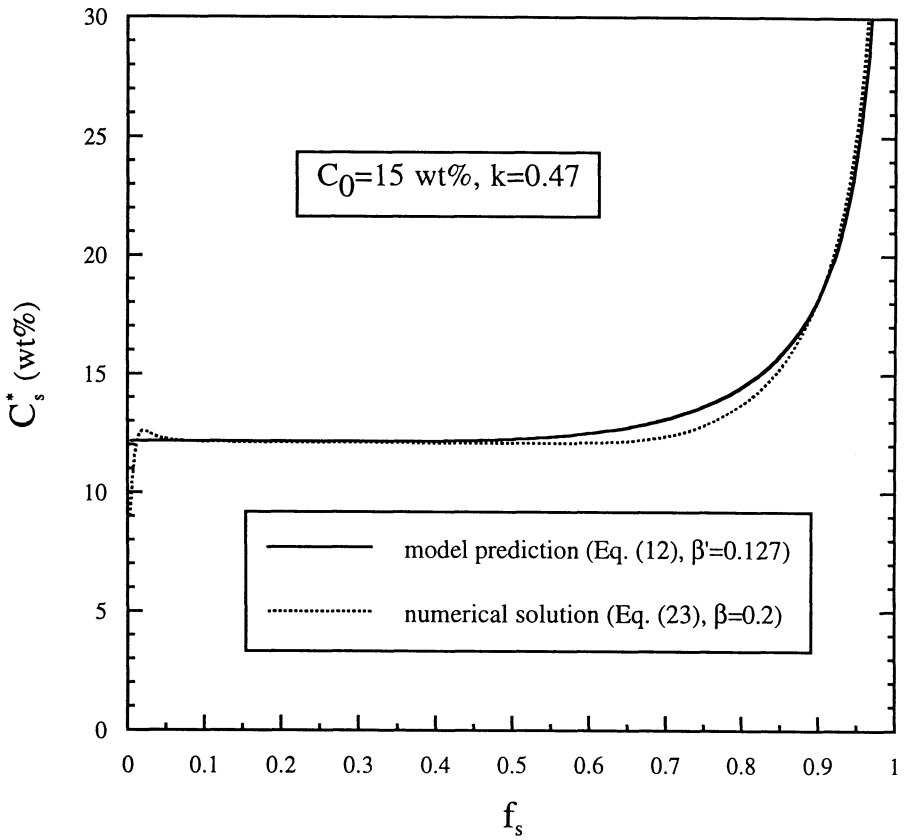

Fig. 6. Comparison of the microsegregation profile predicted by the present model with a numerical solution of the one-dimensional diffusion equation; the parameter β' was chosen to provide a good match between the two profiles.

closely match the numerical solution of Eq. (23). In the case of Fig. 6 ($\beta = 0.2$), the value of the resulting tuning constant is $\sigma = \beta'/\beta = 0.635$. The close agreement in the microsegregation profiles at any solid fraction indicates that the assumed quasi-steady, semi-infinite (exponential) liquid solute profile is a reasonable choice. Because the tuning constant is close to unity, transient and finite domain size effects are not too important.

Fig. 7 shows the variation of the tuning constant σ with the parameter β for $C_0 = 15\%$ and $k = 0.47$. It can be observed that the tuning constant σ varies from 0.3 to 0.75 in the range of $10^{-2} < \beta < 10$. Nevertheless, it can be approximated by a constant value of 0.5 for most purposes. This approximation was found to hold also for other initial concentrations and partition coefficients. The fact that an approximately constant value of σ can be utilized for the entire range of β, shows that the present model is useful not only for rapid solidification, but also for conventional solidification when the liquid approaches a well-mixed state.

3.5. A validation example

One of the rapid solidification experiments of Bendersky and Boettinger [27] is used as a validation example. They measured the microsegregation profile across the cellular structure of an Ag-15 wt%Cu alloy rapidly solidified with a tip speed of 0.12 m/s. The same experiment has also been used by Giovanola and Kurz [18] and Wang and Beckermann [21] to validate their models. As discussed above, the most important issue in applying and validating the present microsegregation model is the evaluation of the liquid diffusion Fourier number, β'. There are two independent methods for evaluating β': (i) through its definition given by Eq. (5b) and (ii) using Eq. (22) and a general tip growth law. Both methods were tried and gave essentially the same value for β'. The latter method is preferred, because it does not require the knowledge of the spacing L and the local solidification time, t_f (although they can be estimated for the conditions in Ref. [27]).

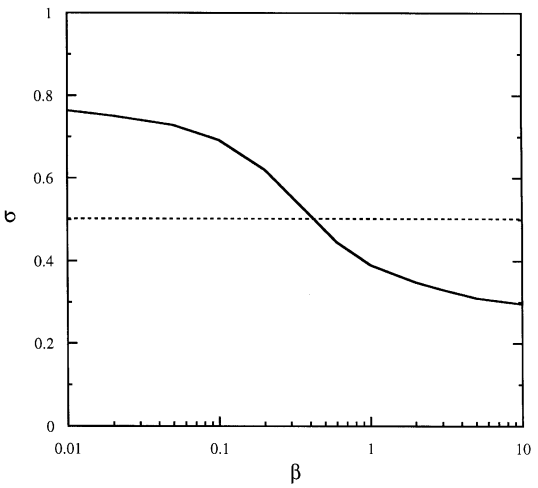

Fig. 7. Variation of the tuning constant, σ, with the solutal Fourier number, β.

In comparison with the experiment, it is important to take into account the temperature and concentration dependence of the thermophysical properties (such as D_l) and the nonlinear nature of the equilibrium phase diagram for Ag–Cu. Using the data and relations provided in Ref. [16] results in the following values of the governing parameters in the experiment of Bendersky and Boettinger [27] ($C_0 = 15$ wt%, $V_t = 0.12$ m/s): $k = 0.588$, Pe $= 1.953$, Iv(Pe) $= 0.718$, and $C^*_{st} = 12.52$ wt%. Hence, with Eq. (22), the Fourier number is $\beta' = 0.196$. As a first approximation, the interface velocity dependent partition coefficient, k, is evaluated at the tip velocity and assumed constant in order to allow for a direct comparison with the results in Ref. [18,21]. Also note that the modification of the original KGT model [16] according to the theory of Boettinger et al. [30] leaves the above predicted tip concentration essentially unchanged [31].

Fig. 8 shows a comparison between the predictions of the present model with the experimental data [28]. The predictions of Giovanola and Kurz [18,19] and Wang and Beckermann [21], as well as the Scheil model and microsegregation-free results, are also included in the figure for comparison. The general features of the microsegregation profile were already discussed in connection with Fig. 3. In general, the agreement between the experiment and the various models can be considered reasonably

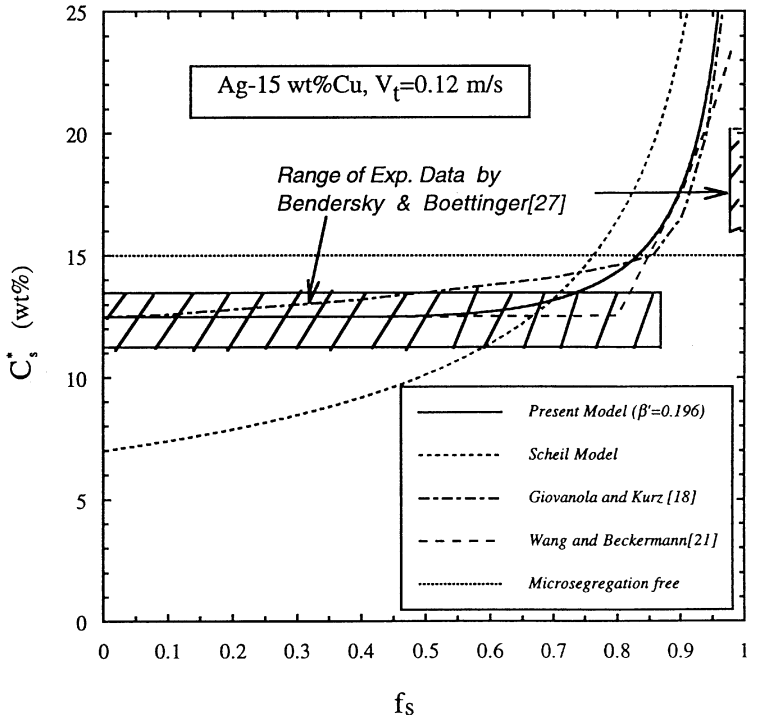

Fig. 8. Comparison of the present microsegregation model with experimental data [27] and other theories [18,21].

good. The present model agrees better with the measurements for solid fractions below 0.75 than the Giovanola and Kurz model. For all solid fractions, it agrees closely with the more complicated model of Wang and Beckermann.

3.6. A correlation for the primary dendrite arm spacing λ_1

As discussed by Hunt and Lu [23], the minimum stable spacing of both cells and dendrites can be determined by considering the so-called *array stability limit*. This limit is determined by the direction of the lateral solute transport at the symmetry line between neighbouring cells/dendrites. Because the present model considers solute transport in the direction perpendicular to the primary growth direction, it is reasonable to expect that a spacing relation can be derived. For simplicity, we consider only dendrites.

For directional solidification, the local solidification t_f can be estimated from the following equation [3],

$$t_f = \frac{\Delta T}{|\dot{T}|}, \tag{27}$$

where ΔT is the freezing temperature range of the mushy zone and $\dot{T}$ is the local cooling rate which is equal to the product of the temperature gradient, G, and the tip velocity, V_t. Combining the asymptotic result [Eq. (22)] with the definition of the parameter β' [Eq. (5b)] and Eq. (27), and using the KGT dendrite tip growth model [16,30], a relation can be derived for the primary dendrite arm spacing $\lambda_1 (= 2L)$ as

$$\lambda_1 = C(\mathrm{Pe}, k)(\Delta T)^{1/2} \left(\frac{\Gamma D_l}{k \Delta T_0}\right)^{1/4} G^{-1/2} V_t^{-1/4}, \tag{28}$$

where

$$C(\mathrm{Pe}, k) = 2\sqrt{\sigma\pi}\left[\frac{1-(1-k)\mathrm{Iv}(\mathrm{Pe})}{\xi_c}\right]^{1/4} \times \left[\frac{2\mathrm{Iv}(\mathrm{Pe})}{1-\mathrm{Iv}(\mathrm{Pe})\mathrm{Pe}}\frac{1}{\mathrm{Pe}}\right]^{1/2}, \tag{29}$$

and $\xi_c = \xi_c(\mathrm{Pe}, k)$ is a correction factor for large tip Peclet numbers and is also provided in Ref. [16]. The temperature interval ΔT_0 is given by $\Delta T_0 = mC_0(k-1)/k$ and Γ is the Gibbs–Thompson coefficient. Eq. (28) is written, on purpose, in a form that is consistent with the standard arm spacing correlations proposed by Hunt [32] and Kurz and Fisher [33]. The only difference with their correlations is the coefficient $C(\mathrm{Pe}, k)$, for which Hunt proposed a constant of 2.83 and Kurz and Fisher proposed 4.3. The value of the constant in the present relation for $C(\mathrm{Pe}, k)$ could be slightly adjusted to account for more realistic dendrite array geometries (e.g., hexagonal or square).

The variation of the coefficient $C(\mathrm{Pe}, k)$ with Pe and k, according to Eq. (29) (with $\sigma = 0.5$), is plotted in Fig. 9. It can be seen that $C(\mathrm{Pe}, k)$ falls roughly into the same range as the constant values proposed in the past [32,33]. The coefficient depends only weakly on the Peclet number for $1 < \mathrm{Pe} < 10$, especially for small k. For $\mathrm{Pe} \to 0$ (i.e., $\beta \to \infty$, well-mixed liquid), the present arm spacing correlation appears to break down; i.e., an infinitely large spacing is predicted. This is not surprising, because the arm spacing is controlled by the interactions between the solute diffusion fields in the liquid from neighbouring arms, which may not be accurately resolved by the present model when the liquid approaches a well-mixed state. Note that for tip Peclet numbers above 0.01 and below 10, the present coefficient $C(\mathrm{Pe}, k)$ is still below 6 (see Fig. 8). For the large spacings predicted for Pe approaching zero, the neglect of dendrite side arms will also make the present analysis inapplicable.

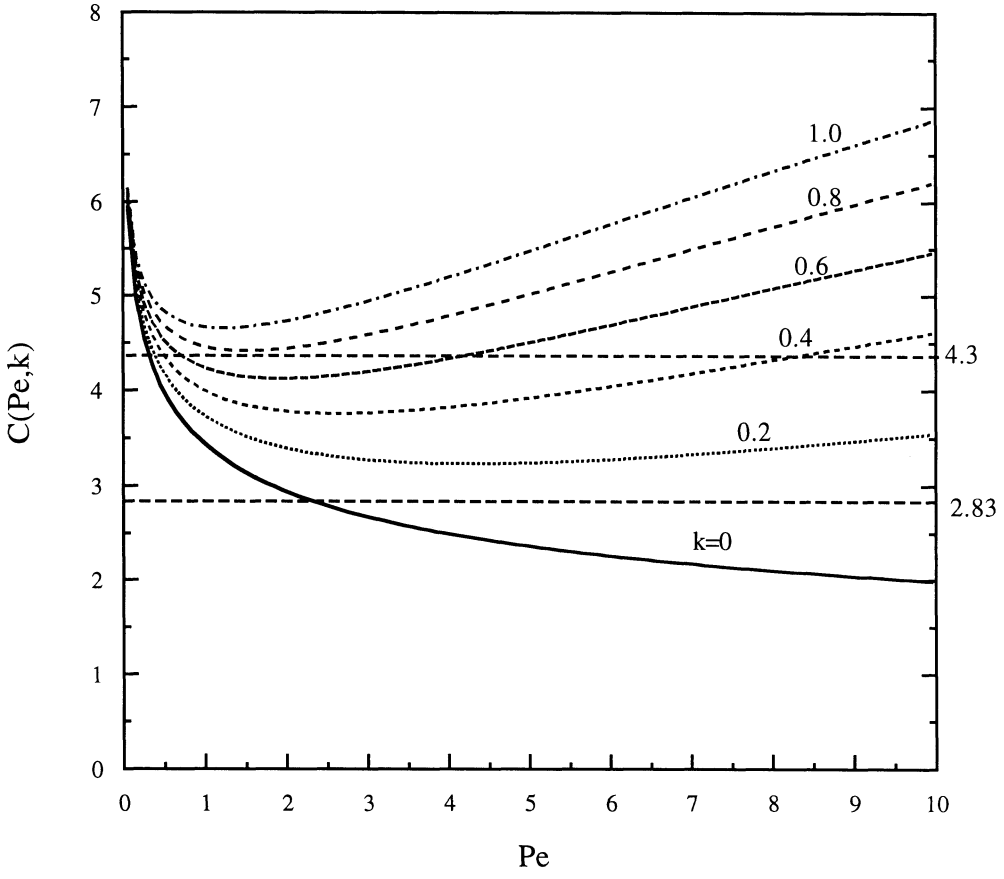

Fig. 9. Coefficient $C(\mathrm{Pe}, k)$ as a function of the tip Peclet number, Pe, and the partition coefficient, k ($\sigma = 0.5$).

The dependence of $C(\mathrm{Pe}, k)$ on k is quite interesting: $C(\mathrm{Pe}, k)$ can be correlated with k^n, where n varies from 0 to almost 0.5 with increasing Pe number. Hunt and Lu [23] showed that a properly defined dimensionless spacing is independent of k, if a certain dimensionless growth velocity and temperature gradient are used in the correlation. Using the same dimensionless parameters in Eq. (28), it can be shown that the coefficient $C(\mathrm{Pe}, k)$ should, in fact, vary with $k^{0.5}$ for the *dimensionless* spacing to be independent of k. Therefore, the seemingly strong dependence of $C(\mathrm{Pe}, k)$ on k for $\mathrm{Pe} > 1$ is in accordance with their study [23]. The variation of the exponent n with Pe in the present study is plausible because the dimensionless counterpart of Eq. (28) is different in form from the arm spacing correlation proposed in Ref. [23].

4. Conclusions

Based on a solute boundary layer analysis, a physically sound microsegregation model is presented that takes into account finite-rate diffusion of solute both in the *solid* and *liquid* phases. Finite-rate diffusion of solute in the liquid phase perpendicular to the growth direction is primarily important in rapid solidification processes with significant cell/dendrite tip undercooling. The following conclusions can be drawn:

1. The input parameters to the present model (in addition to the alloy properties C_0 and k) are the two solutal Fourier numbers α and β. The solid back-diffusion parameter α is in common with other microsegregation models, while β is new and characterizes the extent of solute diffusion in the liquid phase ahead of the solid/liquid interface.
2. The parameter β can be evaluated either through its definition, Eqs. (5a) and (5b) or from Eq. (22) through the knowledge of the operating point of the dendrite tip. It is shown that β uniquely defines the tip operating point.
3. The model equation, Eq. (12), is easily solved and incorporated in standard solidification simulation codes without the need for special procedures. As opposed to the "truncated Scheil" method, it will provide for a "smooth" release of latent heat in the tip region.
4. The present model covers the entire solidification rate spectrum and reduces to the relevant limiting cases.
5. The model predictions are validated with available experimental data and previous analyses.
6. The primary dendrite arm spacing relation based on the present model [Eq. (28)] is in reasonable agreement with previous correlations.

A microsegregation model, based on the same solute boundary layer concept, that includes liquid phase convection will be presented in the near future.

Acknowledgements

This work was supported by the National Science Foundation (NSF) under Grant No. CTS-9501389. Discussions with Dr. W.J. Boettinger of the National Institute of Standards and Technology (NIST) are greatly appreciated.

References

[1] T.P. Battle, Int. Mater. Rev. 37 (1992) 249.
[2] M.C. Flemings, Solidification Processing, McGraw-Hill, New York, 1974.
[3] W. Kurz, D.J. Fisher, Fundamentals of Solidification, 3rd ed., Trans. Tech. Publications, Aedermannsdorf, Switzerland, 1992.
[4] E. Scheil, Z. Metallkde. 34 (1942) 70.
[5] H.D. Brody, M.C. Flemings, Trans. TMS-AIME 236 (1966) 615.
[6] T.W. Clyne, W. Kurz, Metall. Trans. A 12A (1981) 965.
[7] I. Ohnaka, Trans. Iron Steel Inst. Jpn. 26 (1986) 1045.
[8] S. Kobayashi, Trans. Iron Steel Inst. Jpn. 28 (1988) 728.
[9] H. Jones, Rapid Solidification of Metals and Alloys, The Institution of Metallurgists, London, 1982.
[10] P.R. Sahm, H. Jones, C.M. Adam, Science and Technology of the Undercooled Melt, NATO ASI Series E, No. 114, Nijhoff, Dordrecht, 1986.
[11] P.W. Lee, J.H. Moll, Rapidly Solidified Materials: Properties and Processing, ASM International, Metals Park, OH, 1988.
[12] T.F. Bower, H.D. Brody, M.C. Flemings, Trans. AIME 236 (1966) 624.

[13] M. Solari, H. Biloni, J. Crystal Growth 49 (1980) 451.
[14] M.H. Burden, J.D. Hunt, J. Crystal Growth 22 (1974) 109.
[15] S.C. Flood, J.D. Hunt, Appl. Sci. Res. 44 (1987) 27.
[16] W. Kurz, B. Giovanola, R. Trivedi, Acta. Metall. 34 (1986) 823.
[17] U.R. Kattner, W.J. Boettinger, S.R. Coriell, Z. Metallkde. 87 (1996) 522.
[18] B. Giovanola, W. Kurz, Metall. Trans. A 21 (1990) 260.
[19] B. Giovanola, W. Kurz, Z. Metallkde. 82 (1991) 83.
[20] M.C. Flemings, Metall. Trans. A 22 (1991) 957.
[21] C.Y. Wang, C. Beckermann, Mater. Sci. Eng. A 171 (1993) 199.
[22] S.-Z. Lu, J.D. Hunt, J. Crystal Growth 122 (1992) 17.
[23] J.D. Hunt, S.-Z. Lu, Metall. Trans. A 27 (1996) 611.
[24] B.J. Spencer, H.E. Huppert, Acta. Metall. 45 (1997) 1535.
[25] H. Schlichting, Boundary-Layer Theory, 7th ed., McGraw-Hill, New York, 1979.
[26] M.J. Aziz, J. Appl. Phys. 53 (1982) 1158.
[27] L.A. Bendersky, W.J. Boettinger, in: The 5th Int. Conf. on Rapidly Quenched Metals, Wurzburg, Germany, 3–7 September 1984.
[28] G. de Vahl Davis, Numerical Methods in Engineering and Science, Allen & Unwin, London, 1986.
[29] X. Tong, J.A. Khan, S. Dutta, in: ASME HTD 323, Houston, TX, August, 1996, p. 39.
[30] W.J. Boettinger, S.R. Coriell, R. Trivedi, in: R. Mehrabian, P.A. Parrish (Eds.), Rapid Solidification processing: Principles and Technologies, Claitor's Publishing, Baton Rouge, LA, p. 13.
[31] W. Kurz, B. Giovanola, R. Trivedi, J. Crystal Growth 91 (1988) 123.
[32] J.D. Hunt, Solidification and Casting of Metals, Metal Society, London, 1979, p. 1.
[33] W. Kurz, D.J. Fisher, Acta. Metall. 29 (1981) 11.